International Journal of Mathematical, Engineering and Management Sciences
Vol. 9, No. 2, 267-282, 2024
https://doi.org/10.33889/IJMEMS.2024.9.2.014

Ram Arti Publishers

Influence of Nanofluids on Boundary Layer Flow over an Inclined Stretching Sheet in a Porous Media along with Magnetic Field

Sham Bansal
Department of Mathematics,
D.B.S. (P.G.) College (Dehradun), H.N.B. Garhwal Central University, Uttarakhand, India.
Corresponding author: shambansal2010@gmail.com

Jai Pal
Department of Mathematics,
D.B.S. (P.G.) College (Dehradun), H.N.B. Garhwal Central University, Uttarakhand, India.
E-mail: jaipalsingh.dbs@gmail.com

Mangal Singh Bisht
Applied Science and Humanities Department,
Govind Ballabh Pant Institute of Engineering and Technology, Pauri Garhwal, Uttarakhand, India.
E-mail: drbishtms@gmail.com

Prachi Fartyal
Department of Mathematics,
Government P.G. College, Bazpur, U.S. Nagar, Uttarakhand, India.
E-mail: prachifartyal@gmail.com

(Received on November 24, 2023; Revised on January 19, 2024 & February 4, 2024; Accepted on February 6, 2024)

Abstract
The current study intends to analyse the magnetohydrodynamics boundary layer flow of a water-based nanofluid of Silver, Copper and Ferrous Ferric Oxide nanoparticles over a Permeable inclined stretched sheet in a porous media. A similarity transformation is utilized to convert the governing partial differential equations into non-dimensional, non-linear ordinary differential equations. The Keller box finite difference implicit approach is then applied to solve these nonlinear equations numerically. The impacts of several parameters, namely, inclination parameter, magnetic parameter, Soret Number, Eckert number and nano particles volume fractionon velocity, temperature and nanoparticle concentration are explored.

Keywords- Magnetohydrodynamics, Nanofluid, Stretching sheet, Porous medium.

1. Introduction

Due to the wide range of technological and commercial applications, magneto hydro dynamic (MHD) fluid analysis has been the topic of many study projects in the last few decades. In the food engineering, production of petroleum, electricity engineering, polymer solutions and polymer melting industries, MHD boundary layer flow and heat transmission are particularly important. Many constitutive equations have been proposed for magnetohydrodynamic fluids to explain their behaviour in porous media. The application of these nonlinear approaches to mathematical models has become increasingly complex. Mathematics, physics, numerical simulation and modelling scientists are facing fascinating difficulties in attempting to develop analytical or numerical answers. A significant number of academics have been interested in the modelling of nonlinear magnetohydrodynamic fluids in porous media. The present research has used the Keller box finite difference implicit model to solve the non-linear equations numerically.

With the availability of a high magnetic field, heat transfer is crucial in a range of applications, including nanotechnology processing, nuclear liquid metal systems and blood flow regulation, among others. Khan et al. (2016) evaluated the influence of multi-layer viscous fluid flow in divergent and convergent channels. The impact of ion slip and hall currents on high magnetic fields has become increasingly important. The joule heating effects produced by electrical flow heating the electrically conducting fluid are also considerable. The research of hydromagnetic convection flows with comparable effects requires a lot of time and effort. Researchers Rao and Mittal (1981) have been utilising the Runge-Kutta technique in a magnetohydrodynamic generator setup to study the incompressible hydromagnetic boundary layer. The advent of nanofluids has marked significant new developments in the area of thermo-fluid mechanics in recent years. Govardhan et al. (2020) explored the nanofluid's flow via a stretched surface, emphasizing the significance of magnetic field effects on fluid flow features along with the consideration of viscous dissipation. Barletta (1998) states that these fluids are suspensions made up of metallic particles of nanoscale size that are selectively used in conventional fluids in order to obtain much higher thermal characteristics. They explained that if the force of the electromagnetic body is high in the processing of MHD generators, the diffusion rate of ions may be ignored. When the study includes both the electron and the ion velocity, ion-lip phenomena are seen, and Ohm's law must be amended appropriately. In addition to the Hall currents, Reddy et al. (2020) were among the first to investigate the impact of the ion-lip in hydromagnetic heat transfer. They demonstrated that the flow may become unstable if the magnetic field parameters are minimal or when the ion-slip and Hall current parameters are large. Norouzi et al. (2013) observed a reversal flow in the existence of strong ion-slip and Hall effects. Strong ion slip has been found to increase temperatures, whereas increasing the Hall parameter reduces temperatures. The Nusselt number grew substantially as the magnetic parameter ascended, but it first increased and then decreased when the ion-lip parameter increased, suggesting that the Nusselt number significantly increased as the magnetic parameter increased. Takhar and Jha (1998) and Elshehawey et al. (2004) carried out additional research into the interplay between Hall and ion-slip current in heat transfer magnetohydrodynamic flows. Many researches and tests were also conducted in the utilisation of electric heating joule in MHD heat transfer systems. Javeri (1975) have released a research paper describing one of the earliest hydromagnetic heat transfer experiments using Joule heating. In the area of thermal input, they examined the impact of Joule heating on the hydromagnetic heat transfer of the laminar parallel channel in a parallel channel arrangement. Amongst other variables, we looked at situations in which the heat flow of the wall was uniform. Aissa and Mohammadein (2005) carried out a new study utilising their results on the effect of Joule's heating. Duwairi (2005) used an electrothermal modelling code for the network and reported results from additional research utilising Joule heating.

For the functioning of many chemical engineering and material processing systems, material porosity is essential. Cleaning systems and filtering systems all utilise porosity in certain ways. The Darcian model was used to investigate the majority of convection fluxes in porous media. While the model is exact at extremely low Reynolds, it does not reflect inertial effects at higher Reynolds. This is the reason why engineers have developed the Forchheimer-extended Darcian model, which can be readily utilised in calculations of boundary layer heat transport and enables the integration of drag force effects in second order. Chen and Ho (1986) have provided excellent research on Darcy-Forchheimer convection through porous media. Internal friction in viscous fluids may cause temperature fields to change, leading to a variety of industries and geophysics, including viscous dissipation effects. Many researches have been performed in both natural and forced convection thermal transmission systems to evaluate the impact of viscous heat on heat transmission. Gebhart and Mollendorf (1969) and Pop and Soundalgekar (1974) have investigated the Hall current on hydro-magnetic flow in porous media. Several researches have been published in recent years on the impact of viscous heat in hydromagnetic heat transmission. Ghosh et al. (2010) investigated an analytic solution of free convection boundary layer flow under a magnetic field.

All the researches have done so far is based on fluidic regimes. Another thing to notice is that it is derived from the theory of liquid kinetics rather than having a real relationship. A number of research papers published in scientific journals have utilised the tangent hyperbolic fluid model. Tangent hyperbolic nanofluid boundary layer flow was numerically invested by Khan et al. (2017). Krishna et al. (2019) explored Buongiorno's nanofluid flow dynamics through a permeable vertical plate, presenting the influence of dual stratification on the fluid flow characteristics. Nadeem and Akram (2009) performed a thorough study of the peristaltic transport on an asymmetrical channel of a hyperbolic tangent fluid. The dynamics of fluid flow over stretching permeable sheets have been extensively investigated by Chaudhary et al. (2019), they revealed insights into the heat transfer mechanisms.

A rising corpus of research has concentrated on magnetohydrodynamic (MHD) boundary layer flows, which involve the movement of heat and mass from the ever-expanding surface of the fluid to surrounding regions. In use of electrically conduction polymers, magnetic fields may be utilised to control heat or mechanical power, which can save money throughout the production process. Prasad et al. (2013) and Zaib et al. (2020) studied the transportation processes of stretched sheet flows in the boundary layer. They simulate boundary layer borders. Many researchers have studied the flow of stretch sheets for many kinds of stretching speeds. Various robust applications were developed in the processing of MTE materials, including microstructure modifications to the heat transfer, heating induction for matrix ceramic composite materials, liquid metal binding, Lorentzian force control of the boundary layer separation and Lorentzian strength control of the boundary layer separation. Kanika et al. (2020) examined the impact of hydrodynamic flow in conjunction with thermal radiation while taking into consideration the Marangoni boundary layer. Li et al. (2005) and Ghosh et al. (2011) discovered that the constant boundary layer flow can be investigated by obtaining a solution that is exponentially dependent on the heat spreading in the extendable direction.

A finite difference approach was utilised to solve non-dimensionalized conservation equations, including details on the stability and convergence properties of the methodology. Several important thermophysical factors influencing the flux characteristics have been extensively examined and findings have been reported. Nanofluids have revolutionized the landscape of heat transfer and fluid dynamics. The motive of this research is to examine the two-dimensional incompressible boundary layer flow of a water-based nanofluid containing silver (Ag), copper (Cu) and ferrous ferric oxide (Fe_3O_4) nanoparticles across an inclined stretched sheet via a porous media. Ag nanoparticles offer unusual features due to their high surface area to volume ratio, such as antibacterial activity, optical properties, coatings for healthcare equipment and electrical conductivity. They have also shown potential in the treatment of cancer and other conditions linked to angiogenesis. Cu nanoparticles have a high thermal and electrical conductivity, which makes them useful for applications such as electronics and catalysis etc. Due to their affordability and biological compatibility, Fe_3O_4 nanoparticles are a potential material for the latest research. They have been utilized in the manufacture of vaccines and antibodies, cell labelling, genetic therapy, medication delivery and data storage devices etc. Rao and Ramreddy (2019) investigates the double-diffusive nano-fluid flow characteristics while encountering an inclined wavy plate via a porous medium and holds significant implications in understanding heat and mass transfer phenomena. Hayat et al. (2015) explored that how a nanofluid might affect a stretching sheet for a first-order chemical process. Hamad (2011) examined the precise solution of nanofluid flow in MHD convection over a stretching sheet.

According to a review of the literature, multiple studies have described the boundary layer flow via a stretched sheet, but few have investigated the flow of nanofluids via a porous media across an inclined stretched sheet along with a magnetic field. The focus of this study is to minimize this gap by comprehensively analysing the intricate interconnections among nanofluid characteristics, magnetic

forces, and porous media effects on boundary layer flow via an inclined stretched sheet. Through this comprehensive analysis, we aim to uncover previously unexplored facets, contributing to an enhanced comprehension of this intricate phenomenon. The basic equations are transformed via a similarity transformation into a set of nonlinearly ordinary differential equations. These algebraic equations are subsequently computed mathematically via the Keller-box finite difference implicit approach. The impacts of crucial factors shaping fluid flow patterns are presented graphically. The mechanical and engineering roles of porous media are included in the current analysis. To facilitate a smooth and comprehensive understanding of our findings, the subsequent sections have been rigorously structured. Section 2 lays the groundwork by presenting the mathematical formulation of the problem. This includes outlining the governing equations that dictate the behaviour of the system, followed by a comprehensive explanation of the chosen computational approach. Section 3 delves into the core of the investigation, presenting and analysing the numerical results obtained. This section also features a dedicated validation study to ensure the accuracy and reliability of the findings. Finally, Section 4 draws insightful conclusions based on the entire investigation.

2. Mathematical Formulation

The objective of this study is to investigate the characteristics of a two-dimensional, incompressible boundary layer flow involving a nanofluid composed of water and nanoparticles such as silver (Ag), copper (Cu) and ferrous ferric oxide (Fe_3O_4).The governing scenario involves an inclined stretching sheet with a linear velocity profile $(u = bx)$ originating from a fixed point, where b is the stretching rate. The temperature of the stretching sheet (T_w) is assumed to remain constant along with a uniform distribution of nanoparticle fraction (C_w) at the stretching surface. The ambient temperature (T_∞) and nanoparticle fraction (C_∞) are assumed to have constant values in the surrounding environment. The porous medium is considered to be uniform and isotropic along with a constant magnetic field (B_0).The current research problem's physical manifestation is illustrated in Figure 1.

The numerical solutions to this problem use the Keller-box finite difference implicit method developed by Keller and Cebeci (1972). This approach is extremely accurate for numerical analysis of various flow problems and is easy to program for coupled highly nonlinear PDEs. This method is widely used in fluid mechanics to solve two-dimensional boundary layer flow problems. Keller's box design has recently grown in popularity, despite the fact that the concept was created nearly five decades ago. The latest uses of this technique include sound thruster flows, aerodynamic aircraft wing flows, steady convective diffusion flows, magnetohydrodynamics, wavy surface flux, aerodynamic fluids, drainage blade flows and rotational flows. Ishak et al. (2008) and Anwar et al. (2017) employed Keller's box scheme to numerically simulate the flow problem that was being considered. Both studies contribute significantly to the understanding of complex fluid dynamics and heat transfer phenomena in nanofluid-based systems.

The scheme has four main steps:

(i) The n^{th} order nonlinear PDEs system is decomposed into system of n ordinary differential equations of first order.
(ii) These 1^{st} order ordinary differential equations are discretized in finite differences.
(iii) The nonlinear algebraic equations that result from the discretization are transformed into linear algebraic equations.
(iv) The block-tridiagonal elimination approach is employed to solve these transformed algebraic equations.

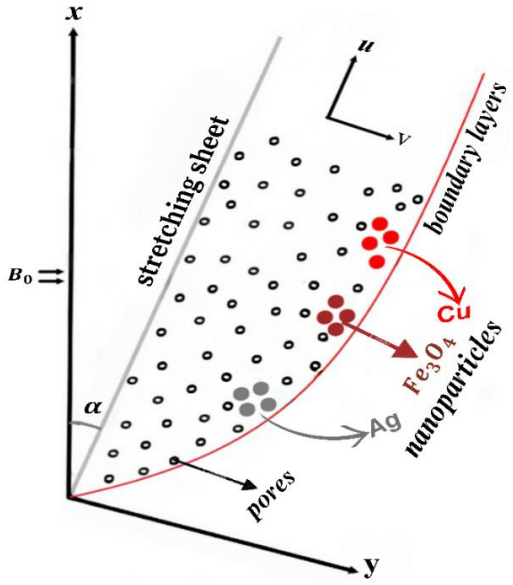

Figure 1. Physical model of present research problem.

The flow problem's related boundary flow equations and boundary conditions are provided by Hayat et al. (2015),

$$\frac{\partial u}{\partial x}+\frac{\partial v}{\partial y}=0 \tag{1}$$

$$u\frac{\partial u}{\partial x}+v\frac{\partial u}{\partial y}=\frac{\mu_{nf}}{\rho_{nf}}\frac{\partial^2 u}{\partial y^2}+g\beta_T(T-T_\infty)Cos(\alpha)+g\beta_C(C-C_\infty)Cos(\alpha)-\frac{\sigma B_0^2}{\rho_{nf}}u-\frac{\mu_{nf}}{\rho_{nf}}\frac{1}{K_d}u \tag{2}$$

$$u\frac{\partial T}{\partial x}+v\frac{\partial T}{\partial y}=\alpha_{nf}\frac{\partial^2 T}{\partial y^2}+\frac{\mu_{nf}}{(\rho C_p)_{nf}}\left(\frac{\partial u}{\partial y}\right)^2 \tag{3}$$

$$u\frac{\partial C}{\partial x}+v\frac{\partial C}{\partial y}=D_m\frac{\partial^2 C}{\partial y^2}+D_l\frac{\partial^2 T}{\partial y^2} \tag{4}$$

$$\left.\begin{aligned}u=u_w=bx, v=v_w, T=T_w \text{ and } C=C_w \text{ at } y=0\\ u=0, T\to T_\infty \text{ and } C\to C_\infty \text{ as } y\to\infty\end{aligned}\right\} \tag{5}$$

The kinematic viscosity v_f, thermal diffusivity α_{nf} and the effective viscosity μ_{nf} for nano-fluids are obtained from (Brinkman, 1952; Maxwell, 1954; Xuan et al., 2003) and are characterized as:

$$\left.\begin{aligned}v_f=\frac{\mu_f}{\rho_f},\ \alpha_{nf}=\frac{\kappa_{nf}}{(\rho C_p)_{nf}},\ \mu_{nf}=\frac{\mu_f}{(1-\phi)^{2.5}},\ (\rho)_{nf}=\left((1-\phi)(\rho)_f+\phi(\rho)_s\right),\\ (\rho C_p)_{nf}=(1-\phi)(\rho C_p)_f+\phi(\rho C_p)_s \text{ and } \frac{\kappa_{nf}}{\kappa_f}=\frac{\kappa_s+2\kappa_f-2\phi(\kappa_f-\kappa_s)}{\kappa_s+2\kappa_f+2\phi(\kappa_f-\kappa_s)}\end{aligned}\right\} \tag{6}$$

Similarity transformations are defined as follows:

$$\eta=y\left(\frac{b}{v_f}\right)^{\frac{1}{2}},\ u=bxf'(\eta),\ v=-(bv_f)^{\frac{1}{2}}f(\eta),\ \theta(\eta)=\frac{T-T_\infty}{T_w-T_\infty} \text{ and } \xi(\eta)=\frac{C-C_\infty}{C_w-C_\infty} \tag{7}$$

Presenting the stream function $\psi(x,y)$, which fulfils the continuity Equation (1) expressed as:

$$u=\frac{\partial\psi}{\partial y} \text{ and } v=-\frac{\partial\psi}{\partial x} \tag{8}$$

From Equation (2) using Equations (6), (7), (8), we get,

$$u\frac{\partial u}{\partial x} = bxf'(\eta).bf'(\eta) = b^2x\left(f'(\eta)\right)^2,$$

$$v\frac{\partial u}{\partial y} = -\left(bv_f\right)^{\frac{1}{2}}f(\eta)\, bxf''(\eta)\left(\frac{b}{v_f}\right)^{\frac{1}{2}} = -b^2xf(\eta)f''(\eta),$$

$$\frac{\mu_{nf}}{\rho_{nf}}\frac{\partial^2 u}{\partial y^2} = \frac{\mu_f}{(1-\phi)^{2.5}} \times \frac{1}{\rho_f\left(1-\phi+\phi\frac{\rho_s}{\rho_f}\right)}\, bxf'''(\eta)\frac{b}{v_f} = \frac{b^2x}{\phi_1\phi_2}f'''(\eta),$$

$$g\beta_T(T-T_\infty) = g\beta_T\theta(\eta)(T_w-T_\infty) \;\; and \;\; g\beta_C(C-C_\infty) = g\beta_C\xi(\eta)(C_w-C_\infty),$$

$$\frac{\sigma B_0^2}{\rho_{nf}}u = \frac{\sigma B_0^2}{\rho_f\phi_2}bxf'(\eta) \text{ and } \frac{\mu_{nf}}{\rho_{nf}}\frac{1}{K_\mathrm{d}}u = v_f\frac{bx}{\phi_1\phi_2}\frac{1}{K_\mathrm{d}}f'(\eta).$$

Now putting the above Equations into (2), we get

$$b^2x\left(f'(\eta)\right)^2 - b^2xf(\eta)f''(\eta) = \frac{b^2x}{\phi_1\phi_2}f'''(\eta) + [g\beta_T\theta(\eta)(T_w-T_\infty) + g\beta_C\xi(\eta)(C_w-C_\infty)]Cos(\alpha) - \frac{\sigma B_0^2}{\rho_f\phi_2}bxf'(\eta) - v_f\frac{b\,x}{\phi_1\phi_2}\frac{1}{K_\mathrm{d}}f'(\eta) \tag{9}$$

Now from (7), we have

$$\left.\begin{aligned} T-T_\infty = \theta(\eta)(T_w-T_\infty) = \theta(\eta)P\left(\frac{x}{l}\right)^2, \text{where P} = (T_w-T_\infty)\left(\frac{l}{x}\right)^2 \\ and \;\; C-C_\infty = \xi(\eta)(C_w-C_\infty) = \xi(\eta)R\left(\frac{x}{l}\right)^2, \text{where R} = (C_w-C_\infty)\left(\frac{l}{x}\right)^2 \end{aligned}\right\} \tag{10}$$

Now from Equation (3) using Equations (6), (7), (8) and (10), we get

$$u\frac{\partial T}{\partial x} = bxf'(\eta)\theta(\eta)\frac{2Px}{l^2} = \frac{2Pbx^2}{l^2}f'(\eta)\theta(\eta),$$

$$v\frac{\partial T}{\partial y} = -\left(bv_f\right)^{\frac{1}{2}}f(\eta)\theta'(\eta)P\left(\frac{x}{l}\right)^2\left(\frac{b}{v_f}\right)^{\frac{1}{2}} = -\frac{Px^2b}{l^2}f(\eta)\theta'(\eta),$$

$$\alpha_{nf}\frac{\partial^2 T}{\partial y^2} = \alpha_{nf}\theta''(\eta)P\left(\frac{x}{l}\right)^2\frac{b}{v_f} = \frac{Px^2b\kappa_{nf}}{l^2v_f\phi_3(\rho C_p)_f}\theta''(\eta),$$

$$\text{and} \quad \frac{\mu_{nf}}{(\rho C_p)_{nf}}\left(\frac{\partial u}{\partial y}\right)^2 = \frac{b^3x^2}{\phi_1\phi_3(C_p)_f}\left(f''(\eta)\right)^2.$$

Now putting the above Equations in (3), we get

$$\frac{2Pbx^2}{l^2}f'(\eta)\theta(\eta) - \frac{Px^2b}{l^2}f(\eta)\theta'(\eta) = \frac{Px^2b\kappa_{nf}}{l^2v_f\phi_3(\rho C_p)_f}\theta''(\eta) + \frac{b^3x^2}{\phi_1\phi_3(C_p)_f}\left(f''(\eta)\right)^2 \tag{11}$$

Now from Equation (4) using Equations (6), (7), (8) and (10), we get

$$u\frac{\partial C}{\partial x} = bxf'(\eta)\xi(\eta)\frac{2Rx}{l^2} = \frac{2Rbx^2}{l^2}f'(\eta)\xi(\eta),$$

$$v\frac{\partial C}{\partial y} = -\left(bv_f\right)^{\frac{1}{2}}f(\eta)\xi'(\eta)\,R\left(\frac{x}{l}\right)^2\left(\frac{b}{v_f}\right)^{\frac{1}{2}} = -\frac{Rx^2b}{l^2}\,f(\eta)\xi'(\eta),$$

$$D_m\frac{\partial^2 C}{\partial y^2} = D_m\xi''(\eta)\,R\left(\frac{x}{l}\right)^2\frac{b}{v_f} = \frac{Rx^2bD_m}{l^2v_f}\xi''(\eta),$$

Ram Arti Publishers

$$\text{and} \quad D_l \frac{\partial^2 T}{\partial y^2} = D_l \theta''(\eta)\, P \left(\frac{x}{l}\right)^2 \frac{b}{\nu_f} = \frac{P x^2 b D_l}{l^2 \nu_f} \theta''(\eta).$$

Now putting the above Equations in (4), we get,

$$\frac{2Rbx^2}{l^2} f'(\eta)\xi(\eta) - \frac{Rx^2 b}{l^2} f(\eta)\xi'(\eta) = \frac{Rx^2 b D_m}{l^2 \nu_f} \xi''(\eta) + \frac{P x^2 b D_l}{l^2 \nu_f} \theta''(\eta) \tag{12}$$

Further simplifying the Equations (9), (11) and (12), we get

$$f'''(\eta) - \phi_1 \phi_2 \left[\left(f'(\eta)\right)^2 - f(\eta) f''(\eta) + \left(Gr_x \theta(\eta) + Gc_x \xi(\eta)\right) Cos(\alpha) \right] - (\phi_1 M - \mathrm{K}) f'(\eta) = 0 \tag{13}$$

$$\theta''(\eta) - Pr \lambda_n^{-1} \phi_3 \left\{ 2f'(\eta)\theta(\eta) - f(\eta)\theta'(\eta) - Ec \phi_1^{-1} \phi_3^{-1} \left(f''(\eta)\right)^2 \right\} = 0 \tag{14}$$

$$\xi''(\eta) - Sc\left(2f'(\eta)\,\xi(\eta) - f(\eta)\xi'(\eta)\right) + \mathrm{Sr}\theta''(\eta) = 0 \tag{15}$$

where, the parameters are

$$\left.\begin{aligned} Pr = \frac{\nu_f}{\alpha_f}, \frac{\kappa_f}{\kappa_{nf}} = \lambda_n^{-1}, \frac{\kappa_f}{\alpha_f} = \left(\rho C_p\right)_f, M = \frac{\sigma B_0^2}{b \rho_f}, Ec = \frac{x^2 b^2}{(T - T_\infty)(C_p)_f}, Gr_x = \frac{g \beta_T (T_w - T_\infty)}{b^2 x}, Gc_x = \frac{g \beta_C (C_w - C_\infty)}{b^2 x}, \\ K = \frac{\nu_f}{b\, K_d}, Sc = \frac{\nu_f}{D_m}, Sr = \frac{(T - T_\infty) D_l}{(C - C_\infty) D_m}, \phi_1 = \frac{1}{(1-\phi)^{2.5}}, \phi_2 = (1 - \phi) + \phi \frac{\rho_s}{\rho_f} \;\&\; \phi_3 = (1 - \phi) + \phi \frac{(\rho C_p)_s}{(\rho C_p)_f} \end{aligned}\right\} \tag{16}$$

In order to achieve similarity solution, Gr_x and Gc_x have to be independent of x. If both the temperature and concentration expansion factors β_T and β_C are proportionalto x, this condition can be met. Hence, one can deduct that $\beta_T = n_1 x$ and $\beta_C = n_2 x$, where n_1 and n_2 are constants, from Makinde and Olanrewaju (2010) and Ilias et al. (2016).

Therefore, from Equation (16), we have

$$Gr = \frac{g n_1 (T_w - T_\infty)}{b^2} \quad \text{and} \quad Gc = \frac{g n_2 (C_w - C_\infty)}{b^2}.$$

To compute the boundary conditions (5), using Equation (7), we get

$$u = u_w = bx \Rightarrow bx f'(\eta) = bx \Rightarrow f'(\eta) = 1,$$

$$v = v_w \Rightarrow -\left(b\nu_f\right)^{\frac{1}{2}} f(\eta) = v_w \Rightarrow f(\eta) = \frac{-\nu_w}{\left(b\,\nu_f\right)^{\frac{1}{2}}} = \mathrm{S},$$

$$T = T_w \Rightarrow T_w - T_\infty = \theta(\eta)(T_w - T_\infty) \Rightarrow \theta(\eta) = 1,$$

$$and \;\; C = C_w \Rightarrow C_w - C_\infty = \xi(\eta)(C_w - C_\infty) \Rightarrow \xi(\eta) = 1.$$

Therefore, the transformed boundary constraints are

$$\left.\begin{aligned} f(\eta) = S,\; f'(\eta) = \theta(\eta) = \xi(\eta) = 1 \;\; at \;\; \eta = 0, \\ and \;\; f'(\eta),\; \theta(\eta) \, and \, \xi(\eta) \to 0 \;\; as \;\; \eta \to \infty \end{aligned}\right\} \tag{17}$$

2.1 Heat Transfer Rate and Skin Friction Coefficient

A dimensionless ratio which characterizes the enhancement of heat transfer in a nanofluid due to convection compared to pure conduction is referred to as Nusselt number. A higher Nusselt Number signifies enhanced convective heat transfer efficiency. Skin friction, refers to the frictional force, generated by fluid's resistance against a solid surface. In boundary layer analysis, it is crucial for understanding the resistance encountered by a fluid moving in contact with a surface. The physical parameters for skin friction $(C_f)$and Nusselt number (Nu) are expressed as:

$$C_f = \frac{\tau_w}{\rho_f u_w^2} \ and \ Nu = \frac{x\, q_w}{\kappa_f (T_w - T_\infty)} \tag{18}$$

where, $q_w = -\kappa_{nf} \frac{\partial T}{\partial y}$ and $\tau_w = \mu_{nf} \frac{\partial u}{\partial y}$ $at\ y = 0$ are energy and shear stress rates.

Finally, the local Nusselt number and the skin friction coefficient are defined as:

$$-\theta'(0) = \frac{\kappa_f}{\kappa_{nf}} Nu(Re_x)^{-1/2} \ and \ C_f(Re_x)^{1/2} = C_{fx}(0) = f''(0), \text{ where } Re_x = \frac{x u_w}{v_f} \tag{19}$$

2.2 Thermophysical Properties of Nanoparticles

The thermophysical characteristics of nanoparticles, including specific heat capacity (C_p), density (ρ), and thermal conductivity (κ), are concisely listed in Table 1. These attributes play a vital role in assessing the nanoparticle's suitability for diverse applications.

Table 1. Thermophysical properties of nanoparticles.

Physical Properties	$C_p(\mathrm{J\,Kg^{-1}K^{-1}})$	$\rho\ (Kg\ m^{-3})$	$\kappa\ (W\ m^{-1}K^{-1})$
$Water\ (H_2O)$	4179	997.1	0.613
Fe_3O_4	670	5180	9.7
Cu	385	8933	401
Ag	235	10500	429

3. Results and Discussion

Employing the Keller-box finite difference implicit approach, numerical computations of non-linear ordinary differential Equations (13-15) having boundary conditions (17) are derived. This study presents a novel approach for effectively visualizing nanofluid flow by utilizing the advanced functionality of MATLAB. This approach not only ensures computational accuracy but also facilitates seamless integration for developing numerical solutions. Using graphs and tables, the impact of various factors, such as, Inclination angle α, Magnetic parameter M, local Grash of number Gr,Suction parameter S, Soret Number Sr, Eckert number Ec, Prandtl number Pr, local modified Grashof numberGc and nanoparticles volume fraction ϕ with nanoparticles Fe_3O_4 ,$Cu\ and\ Ag$ in water based nanofluid are presented.

3.1 Validity of the Present Research

A good research work should be correct scientifically and must pass the validation test. Validity increases transparency and decreases the errors which may affects the accuracy of results. The present research work is validated by referencing prior research conducted by Hamad (2011). In Figure 2 and Table 2, current investigation is reduced to Hamad (2011) model, when $Ec = K = Sr = 0$ and $\alpha = 90^0$, which validate the employed numerical method.

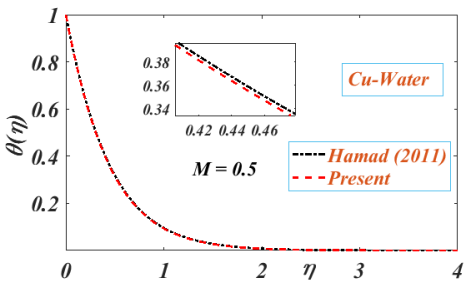

Figure 2. The current investigation is compared to Hamad (2011) modal.

Table 2. Results comparison of the local Nusselt number -$-\theta'(0)$ and skin friction coefficient $-f''(0)$, for distinct values of volume fraction ϕ and the magnetic parameter M, when $Ec = K = Sr = 0$, $Pr = 6.2$ and $\alpha = 90^0$

		$-\theta'(0)$				$-f''(0)$			
		Ag		Cu		Ag		Cu	
M	ϕ	*Hamad* (2011)	*Present*	*Hamad* (2011)	*Present*	*Hamad* (2011)	*Present*	*Hamad* (2011)	*Present*
0	0.05	1.58136	1.581360	1.59899	1.598990	1.13966	1.139664	1.10892	1.108922
0.5	0.1	1.38824	1.388239	1.41848	1.418479	1.37296	1.372963	1.32825	1.328251
1	0.15	1.22994	1.229939	1.27022	1.270219	1.51145	1.511449	1.45858	1.458577
2	0.2	1.07821	1.078210	1.12582	1.125819	1.67583	1.675828	1.62126	1.621256

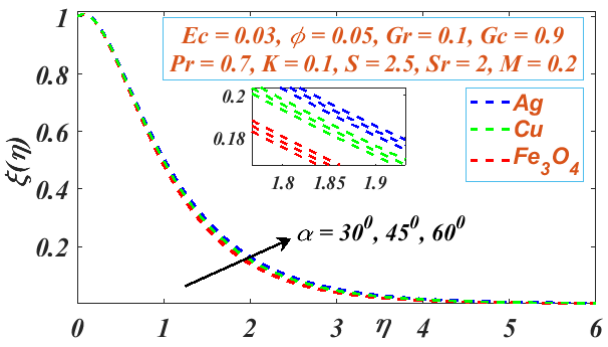

Figure 3. Impact of inclination parameter α on the concentration.

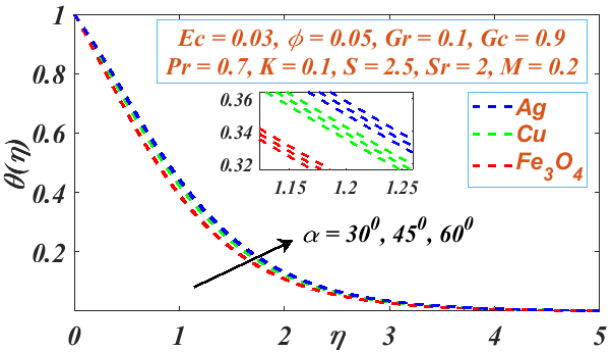

Figure 4. Impact of inclination parameter α on the temperature.

The impact of the inclination angle α on the concentration profile $\xi(\eta)$ is depicted in Figure 3, the $\xi(\eta)$ increases by increasing the angle α. The similar result has been observed for temperature $\theta(\eta)$ in Figure 4 i.e., the temperature rises by increasing inclination angle α. On the other side, opposite effect is observed for velocity $f'(\eta)$ by increasing inclination angle α shown in Figure 5. This kind of behaviour is observed because, if the inclination angle will small then there will be high gravitational force and while increasing the inclination angle, the buoyancy forces become weaker and hence velocity profile decreases. The highest concentration and temperature of nanofluid is observed for nanoparticle Ag followed by Cu and Fe_3O_4 respectively, while highest velocity of nanofluid is observed for nanoparticle Fe_3O_4.

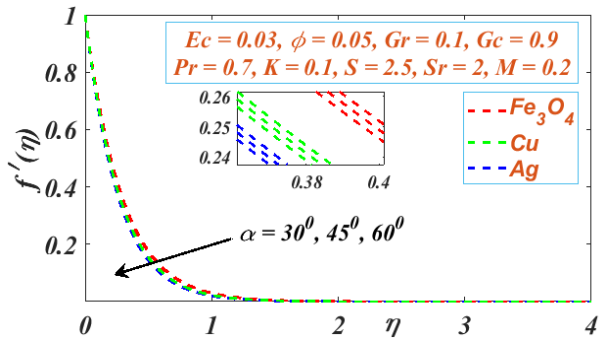

Figure 5. Impact of inclination parameter α on the velocity.

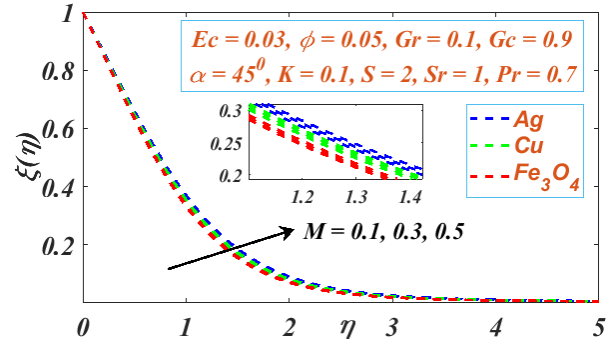

Figure 6. Impact of magnetic parameter M on the concentration.

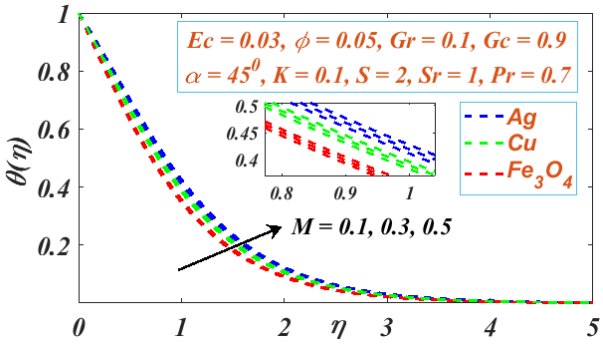

Figure 7. Impact of magnetic parameter M on the temperature.

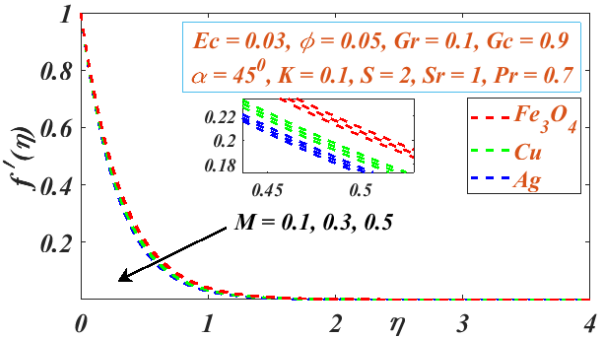

Figure 8. Impact of magnetic parameter M on the velocity.

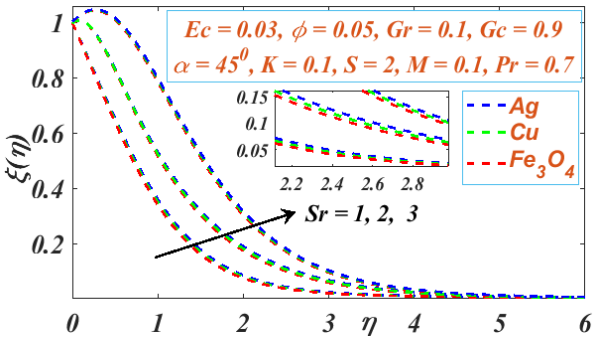

Figure 9. Impact of soret number Sr on the concentration.

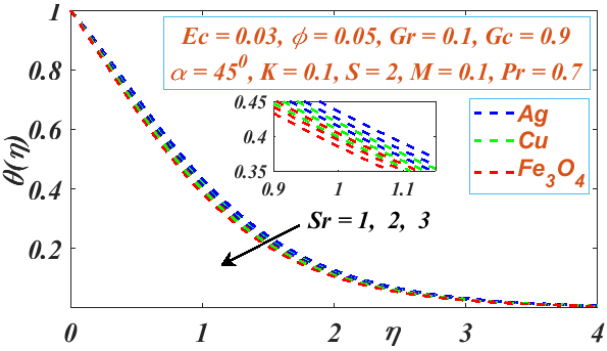

Figure 10. Impact of soret number Sr on the temperature.

The influence of the magnetic parameter M for nanoparticles Fe_3O_4 , $Cu\ and\ Ag$ in water based nanofluid on concentration $\xi(\eta)$ and temperature $\theta(\eta)$ profiles is shown in Figures 6 and 7 respectively, which shows the growth in both Concentration and temperature by enhancing Magnetic parameter M and their boundary layer thickness reaching its maximum at $M = 0.5$. The Lorentz force induces a distinctive drift in charged species, which intricately shapes the concentration profiles. Meanwhile, charged particles interact with the magnetic field to cause localized heating, profoundly altering the thermal characteristics of the nanofluid. In the same vein, opposite result is obtained for velocity $f'(\eta)$ shown by Figure 8. It is because, the magnetic field's Lorentz force, causes resistance in liquid velocity. The highest velocity of nanofluid is noticed for nanoparticle Fe_3O_4 followed by $Cu\ and\ Ag$. Also, at $M = 0.5$, the momentum boundary layer thickness is minimum.

Figures (9-11) demonstrates the considerable effect of Soret parameter Sr on $\xi(\eta), \theta(\eta)$ and $f'(\eta)$. The ratio of a fluid's temperature gradient to concentration gradient is measured by the dimensionless Soret parameter. A rise in the Soret parameter leads to a rise in the fluid's concentration and velocity, a drop in the temperature of the fluid. This is because the Soret effect causes the particles in the fluid to diffuse from high to low temperature zones. This diffusion process also carries the particles with it, which boosts the fluid's velocity. The Soret parameter also have a different impact on the concentration of several kinds of nanoparticles in a fluid. For example, Ag nanoparticles have a higher Soret coefficient than $Cu\ and\ Fe_3O_4$ nanoparticles. This means that Ag nanoparticles will diffuse from areas of high

temperature to areas of low temperature more quickly than $Cu\ and\ Fe_3O_4$ nanoparticles. The impact of the Sr on $\xi(\eta), \theta(\eta)$ and $f'(\eta)$ is capable of altering fluid's behaviour in a wide range of applications. For instance, the Soret effect can be used to separate different types of particles in a fluid.

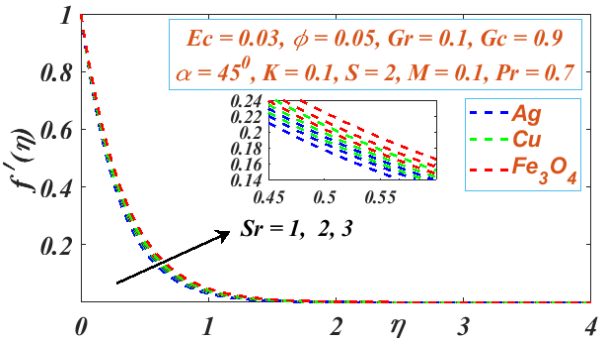

Figure 11. Impact of soret number Sr on the velocity.

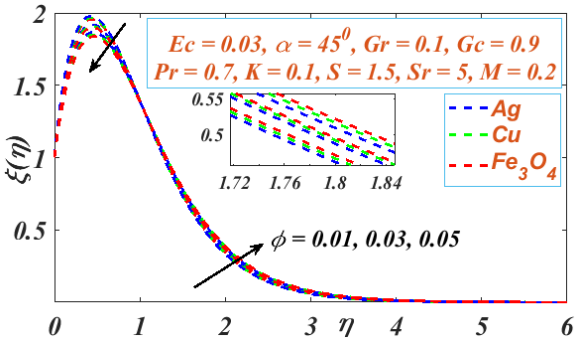

Figure 12. Impact of nano particles volume fraction ϕ on the concentration.

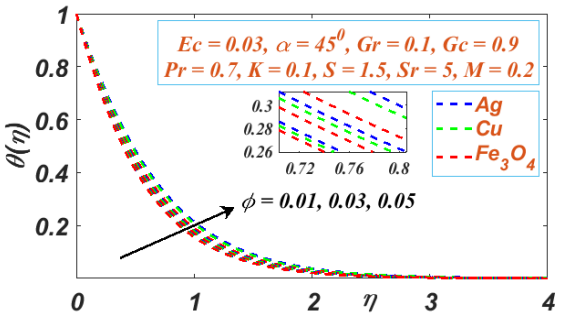

Figure 13. Impact of nano particles volume fraction ϕ on the temperature.

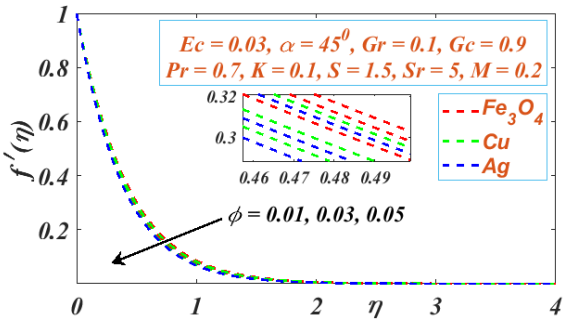

Figure 14. Impact of nano particles volume fraction ϕ on the velocity.

Figures (12-14) demonstrates the significance of nanoparticle volume fraction ϕ on $\xi(\eta), \theta(\eta)$ and $f'(\eta)$ of nanofluids for nanoparticles Fe_3O_4 , $Cu\ and\ Ag$. The nanoparticles volume fraction ϕ is the percentage of the volume of the fluid that is taken up by the nanoparticles. Thermal conductivity of the fluid enhances as the volume fraction ϕ of nanoparticles rises. This results in a rise in the thermal boundary layer of the nanofluid. The velocity profiles of the nanofluid, on the other hand, exhibit the opposite behaviour. The increased viscosity of the nanofluid causes the drop in velocity profile with increasing nanoparticle volume fraction. Though, for concentration $\xi(\eta)$, the concentration profile drops close to the surface $\eta = 0$ and rises at $\eta > 1$ for all three nanoparticles Fe_3O_4 , $Cu\ and\ Ag$, indicating a dual behaviour. Moreover, the concentration of the $Ag\text{-}water$ nanofluid is greater in comparison to the concentration of the $Cu\text{-}water$ and $Fe_3O_4\text{-}water$ nanofluids for $0 < \eta < 1$, whereas reverse behaviour is observed for $\eta > 1$.

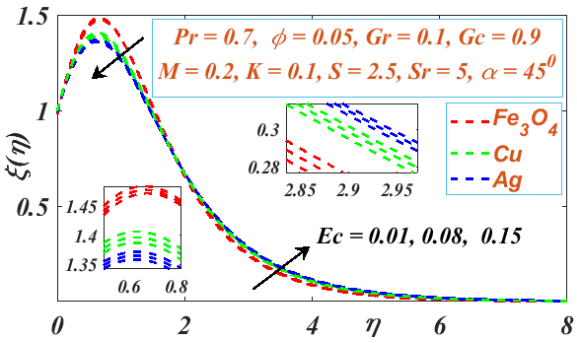

Figure 15. Impact of Eckert number *Ec* on the concentarion.

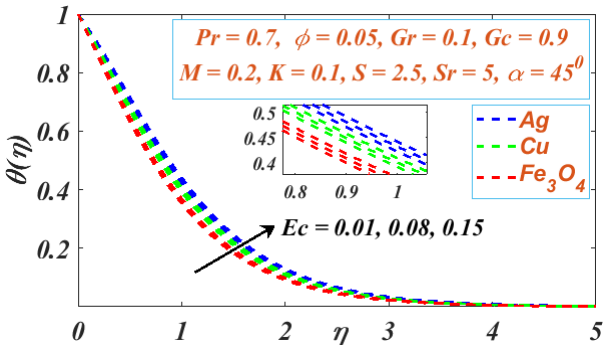

Figure 16. Impact of Eckert number *Ec* on the temperature.

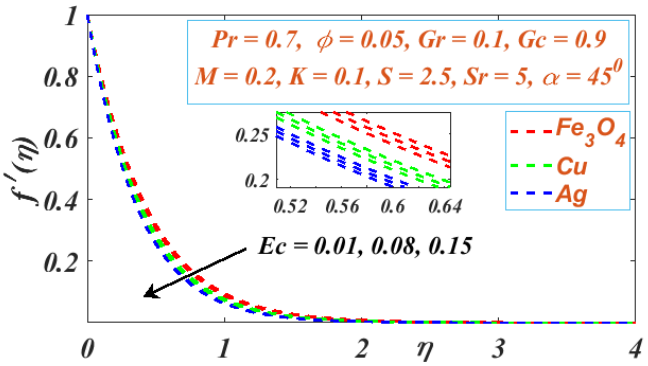

Figure 17. Impact of Eckert number *Ec* on the velocity.

Eckert number (Ec) is a dimensionless parameter, which indicates the kinetic energy to internal energy ratio. The Figures (15-17) show the impact of Ec on concentration, temperature, and velocity distributions for nanofluids containing Fe_3O_4 , Cu and Ag nanoparticles. The concentration of the nanofluid decreases with increasing Ec, but it shows opposite behaviour for $\eta > 1$. The higher Ec values result in a higher temperature, which causes the nanoparticles to diffuse more rapidly away from the wall. This is because the higher Ec values result in a higher kinetic energy, which is transformed into internally generated energy by exerting force against the viscous fluid forces. The velocity of the nanofluid drops by increasing Ec. The impact of Ec on velocity is different for all the three different nanoparticles. For example, the velocity of the Ag-$water$ nanofluid drops more rapidly by increasing Ec than the Cu-$water$nanofluid velocity. The results of this study suggest that Ec is an important parameter to consider when designing nanofluid-based heat transfer applications by carefully selecting the nanoparticle type and value of Ec.

4. Conclusions

The magnetohydrodynamics boundary layer flow of a $water-based$ nanofluid of Ag , Cu and Fe_3O_4 nanoparticles over a permeable inclined stretched sheet in a porous media has been numerically explored. The numerical solutions to this problem use the Keller-box finite difference implicit approach, offering accuracy, stability and efficiency for solving nonlinear boundary layer equations. The approach is easily programmable for highly nonlinear partial differential equations, making it adaptable to the

diverse flow conditions encountered in the present investigation. Some of the interesting findings include;

(i) The temperature $\theta(\eta)$ and concentration $\xi(\eta)$ increases by increasing the angle α, but opposite effect is observed for velocity $f'(\eta)$. The highest concentration and temperature of nanofluid is observed for nanoparticle Ag, followed by Cu and Fe_3O_4 respectively, while highest velocity of is observed for nanoparticle Fe_3O_4.
(ii) Increasing the magnetic parameter increases concentration and temperature and their boundary layer thickness is maximum at $M = 0.5$. In the same vein, opposite result is obtained for velocity $f'(\eta)$. The highest velocity is observed for Fe_3O_4 followed by $Cu\ and\ Ag$.
(iii) Increasing the Soret parameter Srincreases concentration and velocity, and decreases temperature of the fluid. Ag nanoparticles have a higher Soret coefficient than $Cu\ and\ Fe_3O_4$ nanoparticles. The Soret effect can be used to separate different types of particles in a fluid.
(iv) Raising the nanoparticle volume fraction reduces the nanofluid velocity profiles and thickens of the thermal boundary layer. However, concentration reflects dual behaviour: it drops near the surface $\eta = 0$, but rises at a certain distance for all three nanoparticles.
(v) Increasing the Eckart parameter Ec decreases the concentration of the nano fluid near the surface $\eta = 0$, but it shows opposite behaviour for $\eta > 1$. Also, Increasing the Eckart parameter Ec increases the temperature but decreases the nano fluid velocity. The impact of Ec on velocity is different for all the three different nanoparticles. Increasing Ec decreases the Ag-water nanofluid velocity more rapidly than the Cu-water nanofluid velocity.

Conflict of Interest
The authors confirm that there is no conflict of interest to declare for this publication.

Acknowledgments
The authors acknowledge that there has been no financial support for this work that could have influenced its outcome. The authors would like to thank the Editor-in-Chief, section editors and anonymous reviewers for their comments and suggestions that helped them to improve the quality of this work.

Appendix
Symbols and mathematical notations employed throughout this paper, along with their descriptions, are presented in Table 3.

Table 3. Symbols and mathematical notations employed throughout this paper.

Nomenclature		Greek Letter	
B_0	the uniform magnetic field strength	α	inclination parameter
b	Stretching rate	β_T	Thermal expansion coefficient
C	Nanofluid concentration	β_C	Concentration expansion coefficient
C_f	skin-friction	η	non-dimensional similarity variable
C_p	nanoparticle specific heat	κ_f	Base fluid thermal conductivity
C_w	Concentration of the stretching sheet	κ_{nf}	nanofluid thermal conductivity
C_∞	Concentration of the freestream	κ_s	nanoparticles thermal conductivity
D_m	Mass diffusivity	$\theta(\eta)$	non-dimensional temperature
D_t	Mass flux co-efficient	$\xi(\eta)$	non-dimensional concentration
Ec	Eckert number	ϕ	nanoparticles solid volume fraction
$-f''(0)$	skin friction coefficient	σ	Electric conductivity
$f(\eta)$	dimensionless stream function	τ_w	wall shear stress
$f'(\eta)$	Nondimensional velocity	ν_f	Base fluid kinematic viscosity
g	acceleration due to gravity	α_{nf}	nanofluid thermal diffusivity
Gr_x	Local Grash of number	μ_f	Base fluid viscosity

Table 3 continued…

Gc_x	Local modified Grash of number	μ_{nf}	nanofluid viscosity
K	non-dimensional permeability parameter	ρ_f	base fluid density
K_d	dimensional permeability parameter	ρ_{nf}	nanofluid density
l	Characteristic length	ρ_s	nanoparticles density
M	Magnetic parameter	$(\rho C_p)_f$	base fluid heat capacitance
Nu	Nusselt number	$(\rho C_p)_{nf}$	nanofluid heat capacitance
Pr	Prandtl number	$(\rho C_p)_s$	nanoparticles heat capacitance
q_m	wall mass flux	$-\xi'(0)$	local Sherwood number
Re	Reynolds number	$-\theta'(0)$	local Nusselt number
Re_x	local Reynolds number	λ_n	nanofluid thermal conductivity to base fluid ratio
Sr	Soret number	ψ	stream function
Sc	Schmidt number	**Subscripts**	
Sh	Sherwood number		
S	Suction/injection parameter	f	Base fluid
T	dimensional temperature of the nanofluid	w	Boundary conditions at surface
T_w	surface temperature	s	nanoparticles
T_∞	freestream temperature	nf	nanofluid
u	Velocity component parallel to the x direction	∞	boundary conditions at free stream
u_w	Stretching sheet velocity	**Superscripts**	
v	Velocity component parallel to the y direction		
x, y	Cartesian coordinate axis	$'$	differentiation with respect to η

References

Aissa, W.A., & Mohammadein, A.A. (2005). Joule heating effects on a micropolar fluid past a stretching sheet with variable electric conductivity. *Journal of Computational and Applied Mechanics*, *6*(1), 3-13.

Anwar, M.I., Shafie, S., Hayat, T., Shehzad, S.A., & Salleh, M.Z. (2017). Numerical study for MHD stagnation-point flow of a micropolar nanofluid towards a stretching sheet. *Journal of the Brazilian Society of Mechanical Sciences and Engineering*, *39*, 89-100. https://doi.org/10.1007/s40430-016-0610-y.

Barletta, A. (1998). Laminar mixed convection with viscous dissipation in a vertical channel. *International Journal of Heat and Mass Transfer*, *41*(22), 3501-3513. https://doi.org/10.1016/S0017-9310(98)00074-X.

Brinkman, H.C. (1952). The viscosity of concentrated suspensions and solutions. *The Journal of Chemical Physics*, *20*(4), 571-581. https://doi.org/10.1063/1.1700493.

Chaudhary, S., Chaudhary, S., & Singh, S. (2019). Heat transfer in hydromagnetic flow over an unsteady stretching permeable sheet. *International Journal of Mathematical, Engineering and Management Sciences*, *4*(4), 1018-1030. https://dx.doi.org/10.33889/IJMEMS.2019.4.4-081.

Chen, K.S., & Ho, J.R. (1986). Effects of flow inertia on vertical, natural convection in saturated, porous media. *International Journal of Heat and Mass Transfer*, *29*(5), 753-759. https://doi.org/10.1016/0017-9310(86)90126-2.

Duwairi, H.M. (2005). Viscous and Joule heating effects on forced convection flow from radiate isothermal porous surfaces. *International Journal of Numerical Methods for Heat & Fluid Flow*, *15*(5), 429-440. https://doi.org/10.1108/09615530510593620.

Elshehawey, E.F., Eldabe, N.T., Elbarbary, E.M., & Elgazery, N.S. (2004). Chebyshev finite-difference method for the effects of Hall and ion-slip currents on magneto-hydrodynamic flow with variable thermal conductivity. *Canadian Journal of Physics*, *82*(9), 701-715. https://doi.org/10.1139/p04-038.

Gebhart, B., & Mollendorf, J. (1969). Viscous dissipation in external natural convection flows. *Journal of Fluid Mechanics*, *38*(1), 97-107. https://doi.org/10.1017/S0022112069000061.

Ghosh, S.K., Anwar Bég, O., & Zueco, J. (2010). Hydromagnetic free convection flow with induced magnetic field effects. *Meccanica*, *45*, 175-185. https://doi.org/10.1007/s11012-009-9235-x.

Ghosh, S.K., Bég, O.A., & Aziz, A. (2011). A mathematical model for magnetohydrodynamic convection flow in a rotating horizontal channel with inclined magnetic field, magnetic induction and hall current effects. *World Journal of Mechanics, 1*(3), 137-154. https://doi.org/10.4236/wjm.2011.13019.

Govardhan, K., Narender, G., & Sarma, G.S. (2020). Heat and mass transfer in MHD nanofluid over a stretching surface along with viscous dissipation effect. *International Journal of Mathematical, Engineering and Management Sciences*, *5*(2), 343-352. https://doi.org/10.33889/IJMEMS.2020.5.2.028.

Hamad, M.A.A. (2011). Analytical solution of natural convection flow of a nanofluid over a linearly stretching sheet in the presence of magnetic field. *International Communications in Heat and Mass Transfer*, *38*(4), 487-492. https://doi.org/10.1016/j.icheatmasstransfer.2010.12.042.

Hayat, T., Ashraf, M.B., Shehzad, S.A., & Alsaedi, A. (2015). Mixed convection flow of Casson nanofluid over a stretching sheet with convectively heated chemical reaction and heat source/sink. *Journal of Applied Fluid Mechanics*, *8*(4), 803-813. https://doi.org/10.18869/ACADPUB.JAFM.67.223.22995.

Ilias, M.R., Rawi, N.A., & Shafie, S. (2016). MHD free convection flow and heat transfer of ferrofluids over a vertical flat plate with aligned and transverse magnetic field. *Indian Journal of Science and Technology*, *9*(36), 1-7. https://doi.org/10.17485/ijst/2016/v9i36/97347.

Ishak, A., Nazar, R., & Pop, I. (2008). Uniform suction/blowing effect on flow and heat transfer due to a stretching cylinder. *Applied Mathematical Modelling*, *32*(10), 2059-2066. https://doi.org/10.1016/j.apm.2007.06.036.

Javeri, V. (1975). Combined influence of Hall effect, ion slip, viscous dissipation and Joule heating on MHD heat transfer in a channel. *Wärme-und Stoffübertragung*, *8*(3), 193-202. https://doi.org/10.1007/BF01681561.

Kanika, K.M., Chaudhary, S., & Choudhary, M.K. (2020). Influence of magnetic field on thermal radiation and particle shapes of copper-water nanofluid considering Marangoni boundary layer. *International Journal of Mathematical, Engineering and Management Sciences*, *5*(5), 957-970. https://doi.org/10.33889/IJMEMS.2020.5.5.073.

Keller, H.B., & Cebeci, T. (1972). Accurate numerical methods for boundary-layer flows. II: Two dimensional turbulent flows. *American Institute of Aeronautics and Astronautics Journal*, *10*(9), 1193-1199. https://doi.org/10.2514/3.50349.

Khan, M., Hussain, A., Malik, M.Y., Salahuddin, T., & Khan, F. (2017). Boundary layer flow of MHD tangent hyperbolic nanofluid over a stretching sheet: a numerical investigation. *Results in Physics*, *7*, 2837-2844. https://doi.org/10.1016/j.rinp.2017.07.061.

Khan, U., Ahmed, N., & Mohyud-Din, S.T. (2016). Thermo-diffusion, diffusion-thermo and chemical reaction effects on MHD flow of viscous fluid in divergent and convergent channels. *Chemical Engineering Science*, *141*, 17-27. https://doi.org/10.1016/j.ces.2015.10.032.

Krishna, P.M., Ramreddy, C., & Rao, C.V. (2019). Effects of double stratification on MHD flow and heat transfer of nanofluid along a permeable vertical plate. *International Journal of Mathematical, Engineering and Management Sciences*, *4*(6), 1362-1372. https://dx.doi.org/10.33889/IJMEMS.2019.4.6-107.

Li, F.C., Kunugi, T., & Serizawa, A. (2005). MHD effect on flow structures and heat transfer characteristics of liquid metal–gas annular flow in a vertical pipe. *International Journal of Heat and Mass Transfer*, *48*(12), 2571-2581. https://doi.org/10.1016/j.ijheatmasstransfer.2004.12.041.

Makinde, O.D., & Olanrewaju, P.O. (2010). Buoyancy effects on thermal boundary layer over a vertical plate with a convective surface boundary condition. *Journal of Fluids Engineering*, *132*(4), 044502. https://doi.org/10.1115/1.4001386.

Maxwell, J.C. (1954). *A treatise on electricity and magnetism*. Dover Publications, Inc., New York.

Nadeem, S., & Akram, S. (2009). Peristaltic transport of a hyperbolic tangent fluid model in an asymmetric channel. *Zeitschrift für Naturforschung A*, *64*(9-10), 559-567. https://doi.org/10.1515/zna-2009-9-1004.

Norouzi, M., Davoodi, M., Bég, O.A., & Joneidi, A.A. (2013). Analysis of the effect of normal stress differences on heat transfer in creeping viscoelastic Dean flow. *International Journal of Thermal Sciences*, *69*, 61-69. https://doi.org/10.1016/j.ijthermalsci.2013.02.002.

Pop, I., & Soundalgekar, V.M. (1974). Effects of Hall current on hydromagnetic flow near a porous plate. *Acta Mechanica*, *20*(3-4), 315-318. https://doi.org/10.1007/BF01175933.

Prasad, V.R., Rao, A.S., Reddy, N.B., Vasu, B., & Bég, O.A. (2013). Modelling laminar transport phenomena in a Casson rheological fluid from a horizontal circular cylinder with partial slip. *Proceedings of the Institution of Mechanical Engineers, Part E: Journal of Process Mechanical Engineering*, *227*(4), 309-326. https://doi.org/10.1177/0954408912466350.

Rao, B.N., & Mittal, M.L. (1981). Magnetohydrodynamic boundary layer on a wedge. *Journal of Applied Mechanics*, *48*, 656-659.

Rao, C.V., & Ramreddy, C. (2019). Double-diffusive natural convective flow of a nanofluid past an inclined wavy plate in a non-darcy porous medium. *International Journal of Mathematical, Engineering and Management Sciences*, *4*(6), 1373-1383. https://dx.doi.org/10.33889/IJMEMS.2019.4.6-108.

Reddy, M.G., Vijayakumari, P., Krishna, L., Kumar, K.G., & Prasannakumara, B.C. (2020). Convective heat transport in a heat generating MHD vertical layer saturated by a non-Newtonian nanofluid: A bidirectional study. *Multidiscipline Modeling in Materials and Structures*, *16*(6), 1669-1689. https://doi.org/10.1108/MMMS-01-2020-0002.

Takhar, H.S., & Jha, B.K. (1998). Effects of hall and ion-slip currents on MHD flow past an impulsively started plate in a rotating system. *Magnetohydrodynamics and Plasma Research*, *8*, 61-72.

Xuan, Y., Li, Q., & Hu, W. (2003). Aggregation structure and thermal conductivity of nanofluids. *American Institute of Chemical Engineers Journal*, *49*(4), 1038-1043. https://doi.org/10.1002/aic.690490420.

Zaib, A., Khan, U., Wakif, A., & Zaydan, M. (2020). Numerical entropic analysis of mixed MHD convective flows from a non-isothermal vertical flat plate for radiative tangent hyperbolic blood biofluids conveying magnetite ferroparticles: dual similarity solutions. *Arabian Journal for Science and Engineering*, *45*, 5311-5330. https://doi.org/10.1007/s13369-020-04393-x.